PCCP
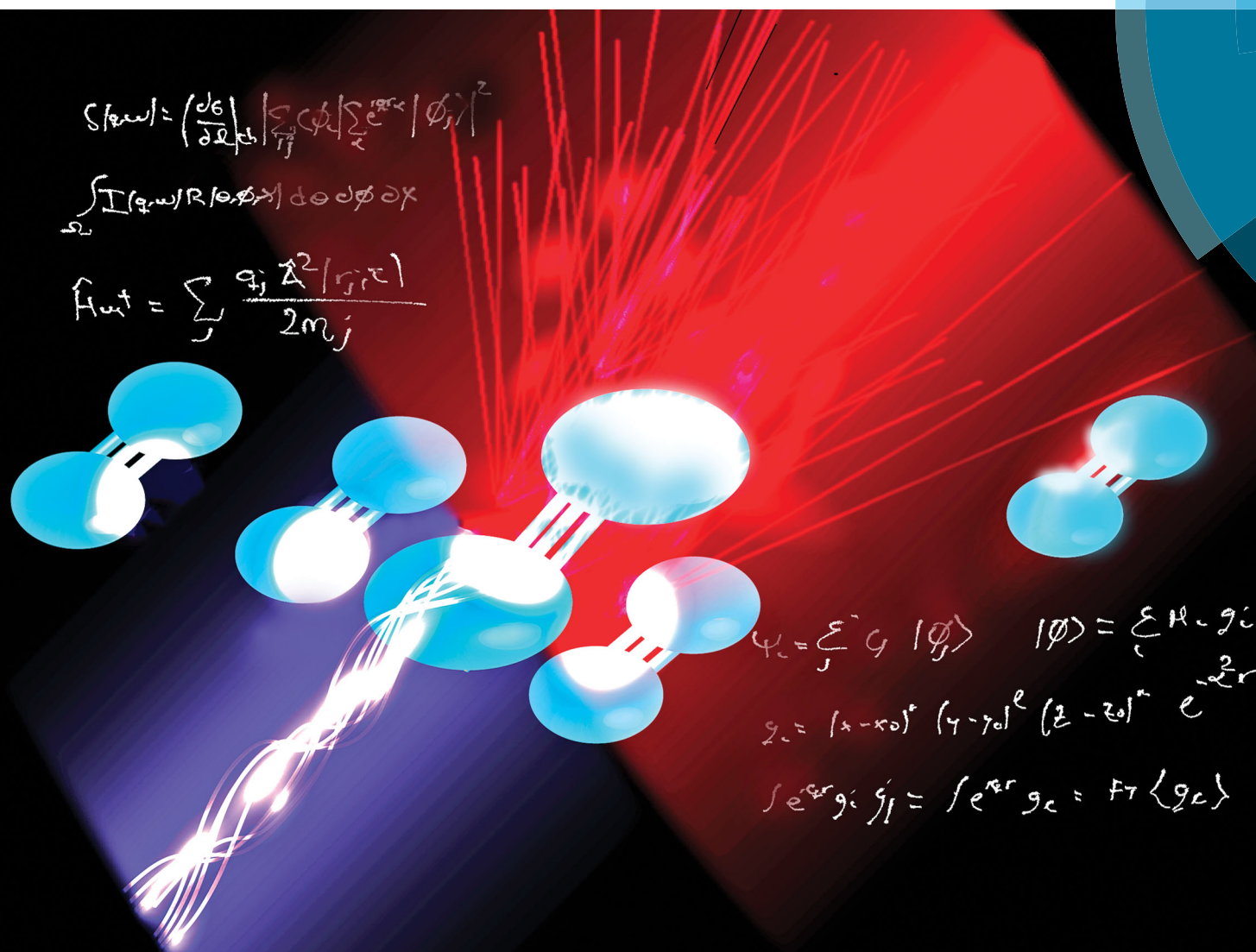
Physical Chemistry Chemical Physics

rsc.li/pccp

Themed issue: XUV/X-Ray light and fast ions for ultrafast chemistry

ROYAL SOCIETY
OF CHEMISTRY

PAPER
Andrés Moreno Carrascosa and Adam Kirrander
Ab initio calculation of inelastic scattering

Check for updates

Ab initio calculation of inelastic scattering

Andrés Moreno Carrascosa and Adam Kirrander ✶

Nonresonant inelastic electron and X-ray scattering cross sections for bound-to-bound transitions in atoms and molecules are calculated directly from *ab initio* electronic wavefunctions. The approach exploits analytical integrals of Gaussian-type functions over the scattering operator, which leads to accurate and efficient calculations. The results are validated by comparison to analytical cross sections in H and He$^+$, and by comparison to experimental results and previous theory for closed-shell He and Ne atoms, open-shell C and Na atoms, and the N_2 molecule, with both inner-shell and valence electronic transitions considered. The method is appropriate for use in conjunction with quantum molecular dynamics simulations and for the analysis of new ultrafast X-ray scattering experiments.

1 Introduction

X-ray scattering has been, and continues to be, instrumental for investigations into the properties of matter. While elastic scattering plays a key role in determining the structure of matter,[1] inelastic scattering enables studies of dynamic properties such as the dispersion of phonons, valence electron excitations, and time-dependent electron dynamics.[2] Recently, new double-differential, high energy-resolution X-ray scattering measurements at synchrotrons have begun to provide an increasingly detailed picture of electronic structure and dynamics in gas-phase atoms and molecules.[3–12] One particular strength of inelastic X-ray scattering (IXS) is the ability to access optically forbidden transitions.

New X-ray Free-Electron Lasers (XFELs), in turn, generate high intensity and short duration pulses[13–19] that enable time-resolved X-ray scattering,[20–25] and thus ultrafast imaging of photochemical dynamics.[26] An attractive feature of such experiments is that they provide direct access to the evolution of molecular geometry *via* the elastic scattering.[27] However, questions remain regarding the degree to which inelastic contributions to the scattering signal can be ignored when analysing experiments, especially in regions where the separation of different electronic states is small.[28–31] For instance, the inelastic contributions are known to be important for imaging of electronic wavepackets in atoms.[32–35] A full theoretical analysis of ultrafast X-ray scattering, beyond the conventional elastic approximation, will require matrix elements corresponding to IXS,[31] which provides an important incentive for the work presented in this article. In addition, it is conceivable that once the appropriate theoretical and computational tools for a more detailed analysis

of ultrafast X-ray scattering experiments are in place, more detailed information can be extracted regarding the electron dynamics that accompanies the structural dynamics of a photochemical process.

In the following, we outline a method for the calculation of IXS from *ab initio* electronic structure calculations in atoms and molecules, based on our previously developed code for the prediction of elastic X-ray scattering.[36–38] An important objective is to match the level of accuracy required for quantum molecular dynamics simulations of photochemical reactions,[31] which generally implies a high-level multiconfigurational description of the electronic structure (*e.g.* CASSCF, CASPT2, or MRCI), while not quite reaching the level of sophistication possible when evaluating IXS from atomic targets or very small molecules (*e.g.* R-matrix theory) in order to maintain a necessary degree of computational efficiency. In the following, we will outline the theory, present our computational approach, and demonstrate that we can calculate IXS accurately.

2 Theory

2.1 X-ray scattering

The total double differential cross section for X-ray scattering is,[2]

$$\frac{d^2\sigma}{d\Omega d\omega_1} = \left(\frac{d\sigma}{d\Omega}\right)_{Th} S(\mathbf{q}, \omega'), \qquad (1)$$

where the strength of the photon–electron coupling is given by the Thomson cross section,

$$\left(\frac{d\sigma}{d\Omega}\right)_{Th} = r_0^2 \left(\frac{\omega_1}{\omega_0}\right) |\mathbf{e}_0 \cdot \mathbf{e}_1^*|, \qquad (2)$$

with $r_0 = e^2/mc^2$ known as the classical electron radius (e is the charge of an electron and c the speed of light), ω_1 and ω_0 the angular frequencies of the scattered and incident X-rays, and $|\mathbf{e}_0 \cdot \mathbf{e}_1^*|$

EaStCHEM, School of Chemistry, University of Edinburgh, David Brewster Road, EH9 3FJ Edinburgh, UK. E-mail: Adam.Kirrander@ed.ac.uk

This journal is © the Owner Societies 2017

Phys. Chem. Chem. Phys., 2017, **19**, 19545–19553 | 19545

the polarization factor. The so-called dynamic structure factor, $S(\mathbf{q}, \omega')$, describes the material response,

$$S(\mathbf{q}, \omega') = \sum_{\beta} \left| \langle \Psi_{\beta} | \hat{L} | \Psi_{\alpha} \rangle \right|^2 \delta\left(E_{\beta} - E_{\alpha} - \hbar \omega' \right), \qquad (3)$$

where $|\Psi_{\beta}\rangle$ and $|\Psi_{\alpha}\rangle$ are the final and initial states, $\omega' = \omega_0 - \omega_1$, and $\hat{L}$ is the scattering operator,

$$\hat{L} = \sum_{j=1}^{N} e^{i\mathbf{q}\mathbf{r_j}}, \qquad (4)$$

with the sum running over all N electrons. The momentum transfer vector, $\mathbf{q} = \mathbf{k}_0 - \mathbf{k}_1$, is defined as the difference between the incident and the scattered wave vectors, with $k_0 = k_1 + \omega'/c$, and $\hbar \omega' = E_{\beta} - E_{\alpha}$ the transition energy, which often is negligible compared to the energy of hard X-rays.[39]

The matrix elements $L_{\beta\alpha} = \langle \Psi_{\beta} | \hat{L} | \Psi_{\alpha} \rangle$ in eqn (3) originate from the $\vec{\mathbf{A}} \cdot \vec{\mathbf{A}}$ terms in the interaction Hamiltonian,[2] where $\vec{\mathbf{A}}$ is the vector potential of the electromagnetic field, at first order of perturbation theory. The competing contributions from the $\vec{\mathbf{p}}\vec{\mathbf{A}}$ terms in the Hamiltonian, which for scattering appear in second order, are sufficiently small to be disregarded.[40] Diagonal matrix elements, $L_{\alpha\alpha} = \langle \Psi_{\alpha} | \hat{L} | \Psi_{\alpha} \rangle$, correspond to elastic scattering and are equivalent to the Fourier transform of the target electron density, a circumstance that underpins the role of elastic scattering in structure determination.[1] Further details regarding the calculation of elastic scattering from *ab initio* wavefunctions can be found in ref. 36 and 41. The remaining off-diagonal, $\alpha \neq \beta$, matrix elements correspond to nonresonant IXS, also referred to as Compton scattering, and are the focus of this article. The elastic and inelastic matrix elements for X-ray scattering, $L_{\beta\alpha}$, are a necessary ingredient in detailed treatments of ultrafast X-ray scattering from non-stationary quantum states by coherent X-ray sources such as XFELs, see *e.g.* ref. 31, and the requirement for these matrix elements is one of the motivations for the work presented in this article.

There is an immediate link between IXS and inelastic scattering of fast charged particles, such as electrons, which has been exploited extensively in Electron Energy-Loss Spectroscopy (EELS).[42] The inelastic scattering of electrons is described by the same matrix elements as IXS,[43,44] although the approximations involved are more severe for electrons than X-rays.[45] Formally, eqn (1) pertains to electron scattering if the Thomson differential cross section, $(dI/d\Omega)_{\text{Th}}$, is replaced by the corresponding Rutherford cross section, $(dI/d\Omega)_{\text{Ru}}$. The scattering elements for elastic electron scattering are not quite identical to X-ray scattering, since they contain additional contributions from electron-nuclei scattering.

The similarity between electron and X-ray scattering in the first Born approximation can be emphasized by the use of generalised oscillator strengths (GOS).[44] In brief, the GOS renormalizes the spectra using the Bethe *f*-sum rule,[43]

$$N = \frac{2}{q^2} \int_0^{\infty} \omega' S(q, \omega') d\omega', \qquad (5)$$

where N is the number of electrons. Such renormalization provides an unitless measure of the strength of spectral features, at a given energy resolution $\Delta\omega$, as,

$$\text{GOS}(q, \bar{\omega}) = \frac{2}{q^2} \int_{\bar{\omega}-0.5\Delta\omega}^{\bar{\omega}+0.5\Delta\omega} \omega' S(q, \omega') d\omega'. \qquad (6)$$

The GOS is often rotationally averaged to account for lack of alignment in the experiments,[44] which explains the usage of q rather than $\mathbf{q}$ in eqn (5) and (6) above. In the literature, a sum over the final degenerate substates and an average over initial Boltzmann-weighted states is frequently implied.

2.2 Scattering matrix elements

An accurate description of excited electronic states in atoms and molecules requires a multiconfiguration expansion of the wavefunction. Simple versions of the one-electron approximation for inelastic scattering are insufficient to describe Compton scattering and multielectron correlation effects must therefore, at least to some extent, be accounted for.[46] In multiconfigurational *ab initio* electronic structure theory the valence electrons are distributed over molecular orbitals in an active space which consists of multiple electron configurations represented by Slater determinants. An electronic state, $|\Psi_{\alpha}\rangle$, can be expanded as,

$$|\Psi_{\alpha}\rangle = \sum_{i=1}^{N_{\text{conf}}} c_{\alpha,i} |\Phi_{\text{SD}}^{\alpha,i}\rangle, \qquad (7)$$

where the $c_{\alpha,i}$ are the configuration interaction coefficients for the electronic state α, N_{conf} is the number of configurations included in the expansion, and $|\Phi_{\text{SD}}^{\alpha,i}\rangle$ are the Slater determinants. The Slater determinants are given by,

$$|\Phi_{\text{SD}}^{\alpha,i}\rangle = (N!)^{-1/2} \sum_{n=1}^{N!} (-1)^{p_n} \mathscr{P}_n \Phi_{\text{H}}^i, \qquad (8)$$

with $\mathscr{P}_n$ the pair-wise permutation operator acting on the Hartree product $\Phi_{\text{H}}^i = \chi_1^i(\mathbf{q_1}) \ldots \chi_N^i(\mathbf{q_{N_e}})$ where $\mathbf{q_j} = (\mathbf{r_j}, \omega_j)$. The spin orbitals $\chi_j^i(\mathbf{q}_j)$ are the products of the spin functions, $|\uparrow\rangle$ or $|\downarrow\rangle$, and the orthonormal spatial molecular orbitals, $\phi_j(\mathbf{r}_j)$, used to construct each Slater determinant.†

Scattering matrix elements $L_{\beta\alpha}$ between electronic states β and α are thus given by,

$$\langle \Psi_{\beta} | \hat{L} | \Psi_{\alpha} \rangle = \sum_{ii'} c_{\beta,i}{}^* c_{\alpha,i'} \langle \Phi_{\text{SD}}^{\beta,i} | \hat{L} | \Phi_{\text{SD}}^{\alpha,i'} \rangle, \qquad (9)$$

using the scattering operator $\hat{L}$ from eqn (4). It is worth noting that we do not explicitly decompose the matrix elements into multipole components by applying the Wigner–Eckart theorem to the operator $\hat{L}$ in eqn (4). The multipole expansion has the advantage that it makes it possible to derive selection rules for single atoms[46] or diatomic molecules,[47] but confers significantly less advantage in the general, non-symmetric, case. Importantly, the

---

† Note that for convenience we allow the index j on the spin orbitals χ_j mirror the electron index j on the electrons ($\mathbf{q_j}$), but that the subset of spin orbitals $\{\chi_j\}$ is different for each Slater determinant. For a total set of $2K$ spin orbitals, one can generate $\binom{2K}{N}$ different determinants.

19546 | *Phys. Chem. Chem. Phys.*, 2017, **19**, 19545–19553

This journal is © the Owner Societies 2017

current treatment has the advantage that the full physical value of the matrix element is obtained straight away.

To evaluate the matrix elements, we note that $\hat{L}$ is the sum of one-electron operators, leading to three standard cases for the evaluation of the brackets on the right-hand side of eqn (9).[48] The first case occurs if the two Slater determinants are identical,

$$
\begin{aligned}
\left\langle \Phi_{\mathrm{SD}}^{\alpha,i} \middle| \hat{L} \middle| \Phi_{\mathrm{SD}}^{\alpha,i} \right\rangle &= \sum_{j=1}^{N} \left\langle \chi_j^i \middle| \hat{l} \middle| \chi_j^i \right\rangle = \sum_{j=1}^{N} \left\langle \phi_j^i \middle| \hat{l} \middle| \phi_j^i \right\rangle \\
&= \sum_{j=1}^{N_{\mathrm{MO}}} b_j \left\langle \phi_j^i \middle| \hat{l} \middle| \phi_j^i \right\rangle,
\end{aligned}
\tag{10}
$$

where $\hat{l}$ is the single electron operator corresponding to $\hat{L}$ in eqn (4). In the final line of eqn (10), $b_j \in 0, 1, 2$ is the occupancy number for each spatial orbital in the Slater determinant when running the summation over all unique spatial orbitals, not just those included in that specific determinant. The second case occurs if the two Slater determinants differ by a single spin orbital when arranged in maximum coincidence,

$$
\left\langle \Phi_{\mathrm{SD}}^{\beta,i} \middle| \hat{L} \middle| \Phi_{\mathrm{SD}}^{\alpha,i'} \right\rangle = \left\langle \chi_N^i \middle| \hat{l} \middle| \chi_N^{i'} \right\rangle = \begin{cases} \left\langle \phi_N^i \middle| \hat{l} \middle| \phi_N^{i'} \right\rangle, \\ 0 \end{cases}
\tag{11}
$$

which is nonzero when the spins of χ_N^i and $\chi_N^{i'}$ are parallel, but vanishes *via* $\langle \downarrow | \uparrow \rangle = 0$ otherwise. Finally, if the two Slater determinants differ by more than one spin orbital, the result is always zero.

2.2.1 Evaluation of matrix elements. The next step requires the evaluation of the integrals that contribute to the matrix elements in eqn (3), corresponding to the brackets listed in eqn (10) and (11). These one-electron integrals over spatial orbitals, expressed in a Gaussian basis, can be evaluated analytically as outlined in the following. The molecular orbitals $\phi_j(\mathbf{r}_j)$ are obtained as linear combinations of the basis functions $G_k(\mathbf{r})$,

$$
\phi_j(\mathbf{r}) = \sum_{k=1}^{N_{\mathrm{BF}}} \mathscr{M}_k^j G_k(\mathbf{r}),
\tag{12}
$$

where $\mathscr{M}_k^j$ are the molecular orbital expansion coefficients. The total number of basis functions $G_k(\mathbf{r})$ is N_{BF}, with $j \in N_{\mathrm{MO}} = N_{\mathrm{BF}}$. Each basis function $G_k(\mathbf{r})$, in turn, is a contraction of Gaussian-type orbitals (GTOs), $g_s(\mathbf{r})$, such that,

$$
G_k(\mathbf{r}) = \sum_{s=1}^{n_k} \mu_s^k g_s(r),
\tag{13}
$$

where μ_s^k are the basis set contraction coefficients for the primitive GTOs. A Cartesian Gaussian-type orbital centered at coordinates $\mathbf{r}_s = (x_s, y_s, z_s)$ has the form,

$$
g_s(\mathbf{r}) = \mathscr{N}_s (x - x_s)^{l_s} (y - y_s)^{m_s} (z - z_s)^{n_s} e^{-\gamma_s (\mathbf{r} - \mathbf{r}_s)^2},
\tag{14}
$$

with exponent γ_s, Cartesian orbital angular momentum $L_s = l_s + m_s + n_s$, and normalisation constant $\mathscr{N}_s$,

$$
\mathscr{N}_s = \left(\frac{2}{\pi}\right)^{3/4} \frac{2^{(l_s + m_s + n_s)} \gamma_s^{(2l_s + 2m_s + 2n_s + 3)/4}}{[(2l_s - 1)!!(2m_s - 1)!!(2n_s - 1)!!]^{1/2}},
\tag{15}
$$

where !! denotes the double factorial. The usage of Cartesian GTOs is convenient in the present context, but there is a direct mapping between Cartesian and spherical Gaussians.[49] If spherical Gaussians are used the mathematics of the analytic Fourier transform takes a different form.[50]

The one-electron bracket in eqn (10) and (11) can then be evaluated as,

$$
\begin{aligned}
\left\langle \phi_a \middle| \hat{l} \middle| \phi_b \right\rangle &= \sum_{k_1, k_2}^{N_{\mathrm{BF}}} \mathscr{M}_{k_1}^a \mathscr{M}_{k_2}^b \sum_{s_1, s_2}^{n_{k_1}, n_{k_2}} \mu_{s_1}^{k_1} \mu_{s_2}^{k_2} K_{s_1 s_2}^{k_1 k_2} \\
&\times \mathscr{F}_{\mathbf{r}} \left[g_{s_1 s_2}^{k_1 k_2}(\mathbf{r}) \right](\mathbf{q})
\end{aligned}
\tag{16}
$$

where we use the Gaussian product theorem[51] to rewrite the product $g_{s_1}^{k_1}(\mathbf{r}) g_{s_2}^{k_2}(\mathbf{r})$ as,

$$
g_{s_1}^{k_1}(\mathbf{r}) g_{s_2}^{k_2}(\mathbf{r}) = K_{s_1 s_2}^{k_1 k_2} g_{s_1 s_2}^{k_1 k_2}(\mathbf{r}),
\tag{17}
$$

where $K_{s_1 s_2}^{k_1 k_2} = \exp\left[-\gamma_{s_1}^{k_1} \gamma_{s_2}^{k_2} \left(\mathbf{r}_{s_1}^{k_1} - \mathbf{r}_{s_2}^{k_2} \right)^2 \middle/ \left(\gamma_{s_1}^{k_1} + \gamma_{s_2}^{k_2} \right) \right]$ is the pre-factor and $g_{s_1 s_2}^{k_1 k_2}(\mathbf{r})$ is the new Gaussian centered at $\mathbf{r}_{s_1 s_2}^{k_1 k_2} = \left(\gamma_{s_1}^{k_1} \mathbf{r}_{s_1}^{k_1} + \gamma_{s_2}^{k_2} \mathbf{r}_{s_2}^{k_2} \right) \middle/ \left(\gamma_{s_1}^{k_1} + \gamma_{s_2}^{k_2} \right)$ with exponent $\gamma_{s_1 s_2}^{k_1 k_2} = \gamma_{s_1}^{k_1} + \gamma_{s_2}^{k_2}$. Since the Cartesian coordinates (x, y, z) are linearly independent and each Gaussian function can be written as a product of x, y and z components,

$$
g_{s_1 s_2}^{k_1 k_2}(\mathbf{r}) = \prod_{r'=x,y,z} g_{s_1 s_2}^{k_1 k_2}(r'),
\tag{18}
$$

the problem is reduced to the solution of one-dimensional Fourier transforms $\mathscr{F}_x \left[g_{s_1 s_2}^{k_1 k_2}(x) \right](q)$. These can be determined analytically, as has been shown and tabulated in a previous publication.[36]

3 Computational details

As pointed out in Section 2.2, a correct description of excited electronic states requires multiconfigurational wavefunctions. In the following, we focus on CASSCF, MCSCF, and MRCI level theory, which provides an attractive compromise between computational resources and accuracy, and constitutes a level of theory frequently used in quantum molecular dynamics simulations of small and medium sized molecules.[52–55] The wave functions are calculated using state averaging and the results are expressed using CI configurations, with the weights given by the configuration interaction vector. The calculations are more convenient if the CI vector is expanded over configuration state functions (CSF) instead over individual Slater determinants. In the case of MRCI methods, the calculation is performed using CSF already, expressing the spin populations as branches with only a merely statistical meaning in terms of spin quantum numbers. This gives the inelastic scattering matrix elements as,

$$
\left\langle \Psi_\beta \middle| \hat{L} \middle| \Psi_\alpha \right\rangle = \left| \sum_{i,j}^{N_{\mathrm{CI}}} v_{\beta,i}^{\mathrm{CI}} v_{\alpha,j}^{\mathrm{CI}} \left\langle \Phi_{\mathrm{SD}}^{\beta,i} \middle| \hat{L} \middle| \Phi_{\mathrm{SD}}^{\alpha,j} \right\rangle \right|^2,
\tag{19}
$$

where v_α^{CI} are the CI-vectors of length N_{CI}. Only pairs of Slater determinants that differ by less than two occupied orbitals will give a non-zero result, as discussed earlier, which makes it possible to swiftly filter out null contributions to the integrals. If doublet or triplet states are considered, appropriate prefactors need to be included when spatial orbitals are evaluated. Furthermore, in small systems, such as atoms or diatomic molecules, symmetry is useful to reduce the number of calculations required. We have used the electronic structure package MOLPRO[56] to carry out the *ab initio* calculations, and calculated the IXS cross sections using a new version of our recently developed *ab initio* X-ray diffraction (AIXRD) code.[36]

The IXS cross sections in this article are given in terms of the dynamic structure factor, $S(q,\omega_\beta)$, or the generalized oscillator strength, $GOS(q,\bar\omega)$, with the choice between the two representations determined by the source of the reference data used for comparison. All calculated data is given at perfect energy resolution, *i.e.* with no averaging over energy ($\Delta\omega = 0$ in eqn (6)). The results for Ne and N_2 are rotationally averaged to match published data. Furthermore, the astute reader will notice that some graphs show the cross sections as a function of q, while others as a function of q^2. The choice, again, reflects the source of the reference data, with EELS measurements (or IXS measurements that compare to EELS data) generally shown as a function of q^2 in order to offset the small angle of scattering for EELS.

4 Results and discussion

4.1 Single-electron atoms

We begin by a comparison of analytical and numerical results for the dynamic structure factor, $S(q,\omega)$, in the single-electron atoms H and He$^+$. The analytical results are computed along the lines in ref. 50. Numerically, the wavefunctions are calculated at the CASSCF(1,3) level, which is more than sufficient in the present case, using the Dunning basis d-aug-cc-PV5Z. The d-aug family of basis sets allows a better description of the diffuse orbitals in hydrogen-like atoms when the principal quantum number is $n > 1$, *i.e.* for hydrogenic Rydberg states. The calculated *ab initio* transition energies for $(2s,2p,3s) \leftarrow 1s$ are within $<0.1\%$ of the experimental[57] and analytical result. As apparent from Fig. 1, the analytical and numerical results for $S(q,\omega)$ agree well in both cases, with the dynamic structure factor extending to larger values of q for transitions for the more compact He$^+$ states (Fig. 1b) compared to H (Fig. 1a), as expected.

4.2 Two-electron atoms

We now consider the He atom, a two-electron system. The electronic states of He are well known. The energy convergence for CASSCF(2,10) *ab initio* calculations with four different Dunning basis sets is shown in Table 1 for the two excited states $^1S_0(1s2s)$ and $^1P_1(1s2p)$, with the corresponding dynamic structure factor for the $^1S_0(1s2s) \leftarrow {}^1S_0(1s^2)$ transition from the ground state shown in Fig. 2 together with reference calculations using explicitly correlated wavefunctions by Cann and Thakkar.[58] Agreement between the reference results and our
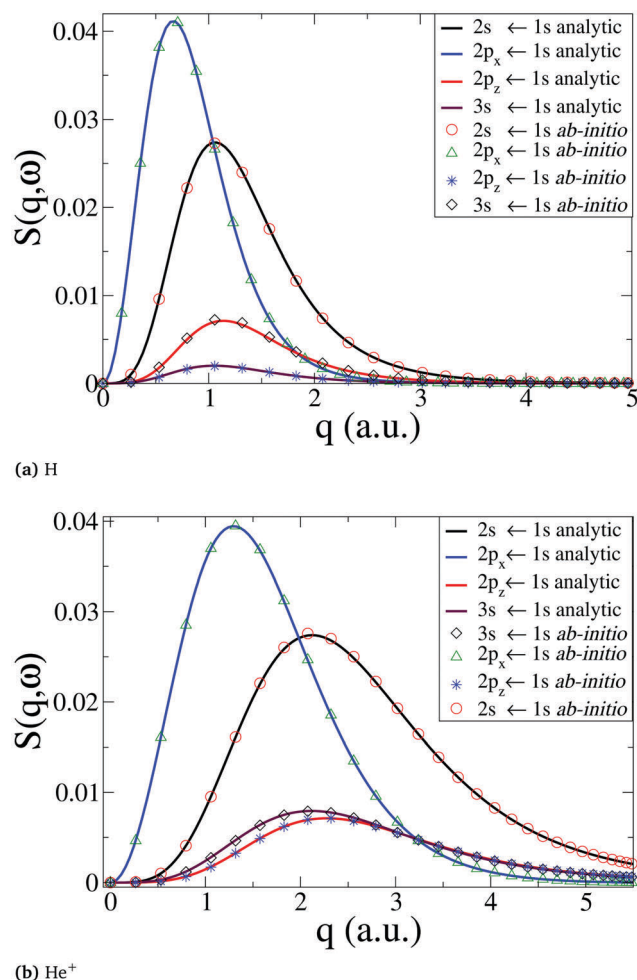

(a) H

(b) He$^+$

Fig. 1 Comparison between numerical *ab initio* calculations, using our approach, and analytical results for (a) the H neutral atom, and (b) the He$^+$ cation. The dynamic structure factor, $S(q,\omega)$, is shown for the transitions $2s \leftarrow 1s$, $2p_x(2p_y) \leftarrow 1s$, $2p_z \leftarrow 1s$, and $3s \leftarrow 1s$.

calculations is good, with the best agreement achieved with the aug-cc-PV6Z basis, which also has the best energy convergence. The remaining discrepancies for the aug-cc-PV6Z basis occur predominantly at small values of q. Importantly, the correlation between energy convergence in Table 1 and the quality of the scattering in Fig. 2, indicate that the calculations are robust and that systematic improvements are possible. The energy convergence is a good predictor of the quality of the calculated

Table 1 Energies E for the $^1S_0(1s2s)$ and $^1P_1(1s2p)$ states in He calculated at the CASSCF(2,10) level with Dunning basis sets: aug-cc-PVQZ, aug-cc-PV5Z, aug-cc-PV6Z, and d-aug-cc-PV5Z. The percentage error, ΔE, compared to experimental values from NIST[57] is also given

He	$^1S_0(1s2s)$		$^1P_1(1s2p)$	
	E (eV)	ΔE (%)	E (eV)	ΔE (%)
Exp.[57]	20.615	—	21.218	—
PVQZ	20.793	0.8	23.943	12.8
PV5Z	20.748	0.6	23.078	8.8
PV6Z	20.684	0.3	22.667	6.8
d-PV5Z	20.000	3.0	20.680	2.5

19548 | *Phys. Chem. Chem. Phys.*, 2017, **19**, 19545–19553
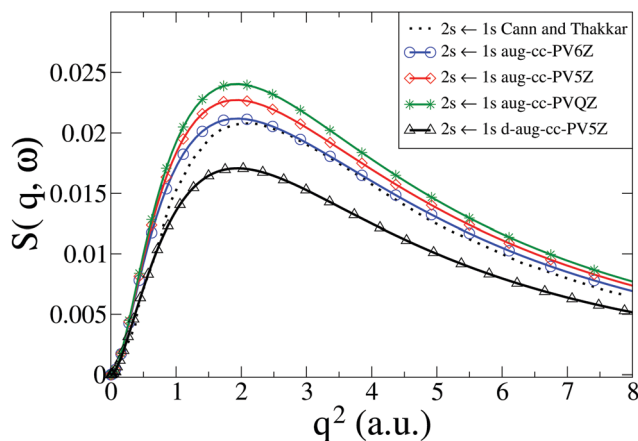
This journal is © the Owner Societies 2017

Fig. 2 Calculated dynamic structure factor, $S(q,\omega)$, in He for the $^1S_0(1s2s) \leftarrow$ $^1S_0(1s^2)$ transition compared to results from Cann and Thakkar.[58] The numerical calculations are performed with CASSCF(2,10) and four Dunning basis sets (aug-cc-PVQZ, aug-cc-PV5Z, aug-cc-PV6Z, and d-aug-cc-PV5Z).

inelastic scattering; we have previously made the same observation for the calculation of elastic scattering matrix elements.[37,38]

In Fig. 3 we compare our calculated dynamic structure factors for the two transitions $^1S_0(1s2s) \leftarrow {}^1S_0(1s^2)$ and $^1P_1(1s2p) \leftarrow {}^1S_0(1s^2)$ in He to experimental results by Xie et al.[7] and reference calculations by Cann and Thakkar.[58] The agreement between present and previous calculations and the experimental data is good, with the reference calculations reproducing experiments slightly better for $q < 2$ a.u. The fact that the energy convergence for the $^1S_0$ state is better than for the $^1P_1$ state in our calculations (see Table 1) appears to have little effect on the agreement between the dynamic structure factor for the two transitions in our calculations and the experimental results, with the convergence of $^1S_0(1s2s) \leftarrow {}^1S_0(1s^2)$ only marginally better than for $^1P_1(1s2p) \leftarrow {}^1S_0(1s^2)$. Notably, for both transitions the best agreement with experimental data is achieved
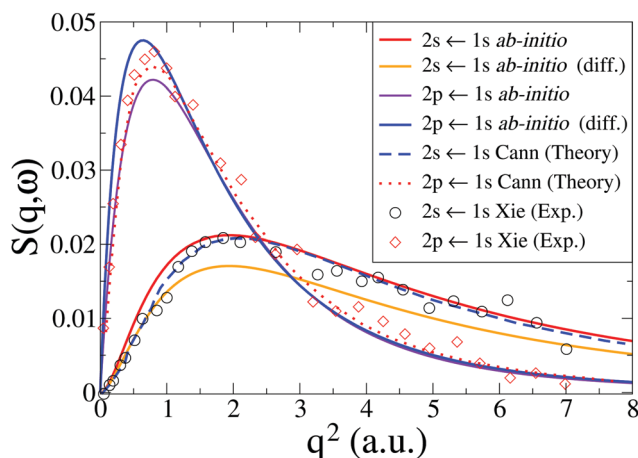
with the basis set that yields the best energy convergence for that state (see Table 1).

4.3 Multi-electron atoms

4.3.1 Ne. The first multi-electron atom that we consider is the closed-shell rare-gas atom Ne, where we investigate inelastic excitations from the outer subshell np⁶ electrons. These have been studied before, theoretically[46,59] and experimentally using both EELS[60] and IXS.[10] The IXS measurements by Zhu et al.[10] demonstrate elegantly that the intensity of the EELS measurements at high q is increased by contamination from high-order Born terms corresponding to multiple scattering. For X-ray scattering, only first-order Born terms contribute due to the weaker interaction.

In the following, we focus the comparison on the previous benchmark random-phase with exchange (RPAE) calculations by Amusia et al.[46] The excitations studied are characterized by the dependency on the total angular momentum, and following the lead of Amusia et al. we discuss the cross sections in terms of the monopole, dipole, and quadrupole transitions, respectively. We perform our ab initio calculations at the CASSCF(10,9)/aug-cc-PVTZ level of theory. Note that when using a general-use ab initio electronic structure package, one has to pay careful attention to symmetry and multiplicity in order to isolate different contributions correctly for an atom. The energies of the excited states of Ne involved in the monopole, dipole, and quadrupole transitions from the ground state are listed in Table 2.

In Fig. 4 we compare our results with those by Amusia et al.[46] for the monopole and quadrupole 3p ← 2p and the dipole 3s ← 2p transitions. Note that the cross sections have been rotationally averaged (see Section 2). Overall, the agreement is very good, with the only notable discrepancy occurring for the dipole 3s ← 2p transition, where the low-q peak in our calculations is marginally shifted to lower values of q compared to Amusia et al., although the height and width of the peak agree almost perfectly. The Amusia et al. calculations have been compared to the recent IXS experiments by Zhu et al.,[10] and the agreement for the monopole $2p^53p[1/2]_0$, the dipole $2p^53s[1/2]_1$, and the quadrupole $2p^53p[5/2,3/2]_2$ were found to be quite good, which carries over to our present calculations.

4.3.2 C and Na. Next we consider two open-shell atoms, C and Na, which provides an opportunity to examine cross sections for inner shell excitations in higher multiplicity systems with unpaired electrons in the ground state and a significant degree of electron correlation. The energy convergence of the CASSCF/aug-cc-PVTZ calculations are shown in Table 3.

Fig. 3 Calculated dynamic structure factor, $S(q,\omega)$, in He for the $^1S_0(1s2s) \leftarrow$ $^1S_0(1s^2)$ and $^1P_1(1s2p) \leftarrow {}^1S_0(1s^2)$ transitions compared to theory by Cann and Thakkar[58] and experiments by Xie et al.[7] The ab initio calculations are done at the CASSCF(2,10)/aug-cc-PV6Z and the CASSCF(2,10)/d-aug-cc-PV5Z levels, with the d-aug results identified by the label "(diff.)".

Table 2 Energies E_{calc} for excited states in Ne atom calculated using CASSCF(10,9)/aug-cc-PVTZ. The percentage error, ΔE, relative experimental values E_{exp} from NIST[57] is also given

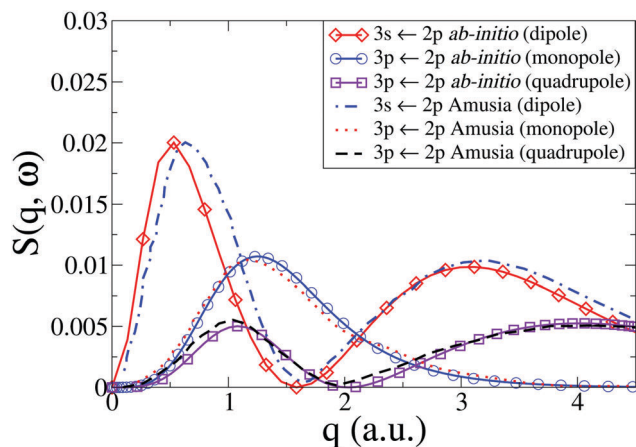| Ne	E_{exp} (eV)	E_{calc} (eV)	ΔE (%)
$2s2p^53s[1/2]_1$	16.715	16.554	1.0
$2s2p^53p[1/2]_0$	18.555	18.290	1.4
$2s2p^53p[3/2]_2$	18.704	18.720	0.1

Fig. 4 Dynamic structure factor, $S(q,\omega)$, in Ne for the $3s \leftarrow 2p$ dipolar and $3p \leftarrow 2p$ monopolar and quadrupolar transitions compared to results by Amusia et al.[46]

Table 3 Energies E_{calc} for excited states in atoms C and Na calculated at the CASSCF/aug-cc-PVTZ level of theory (see text for details). The percentage error, ΔE, compared to experimental values E_{exp} from NIST[57] and Bielschowsky et al.[62] is also given

Atom [state]	E_{exp} (eV)	E_{calc} (eV)	ΔE (%)
C $[2s2p^3\ ^3P]$	9.330^{57}	9.576	2.6
C $[2s2p^3\ ^3D]$	7.946^{57}	7.410	6.7
Na $[2p^53s^2\ ^2P]$	31.200^{62}	31.489	0.9

The IXS cross sections for the transitions from the ground state of the C atom to the first two inner-shell excited states, i.e. $^3P([He]2s2p^3) \leftarrow\ ^3P([He]2s^22p^2)$ and $^3D([He]2s2p^3) \leftarrow\ ^3P([He]2s^22p^2)$, are shown in Fig. 5. Our ab initio calculations, done at the CASSCF(6,5)/aug-cc-PVTZ level, agree well with the RPAE calculations by Chen and Msezane,[61] also included in Fig. 5. For $q^2 \to 0$ the GOSs should converge to the optical oscillator strength of the transitions. In our calculations these values are 0.0615 and
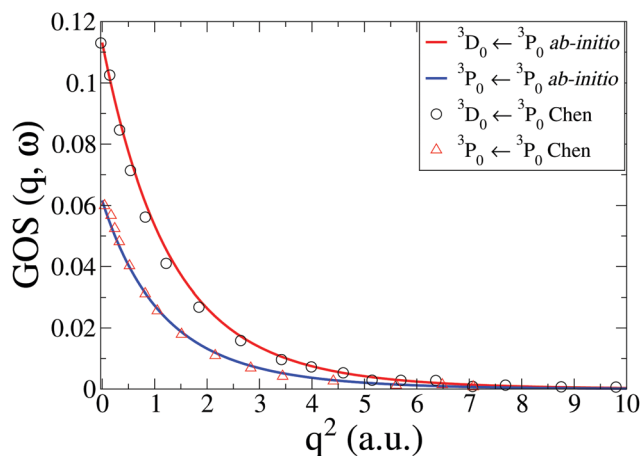

Fig. 5 Generalized oscillator strengths, GOS(q,ω), in C for the two transitions $^3P_0(2s2p^3) \leftarrow\ ^3P_0(2s^22p^2)$ and $^3D_0(2s2p^3) \leftarrow\ ^3P_0(2s^22p^2)$. The current ab initio calculations using CASSCF(6,5)/aug-cc-PVTZ are compared to RPAE calculations by Chen and Msezane.[61]
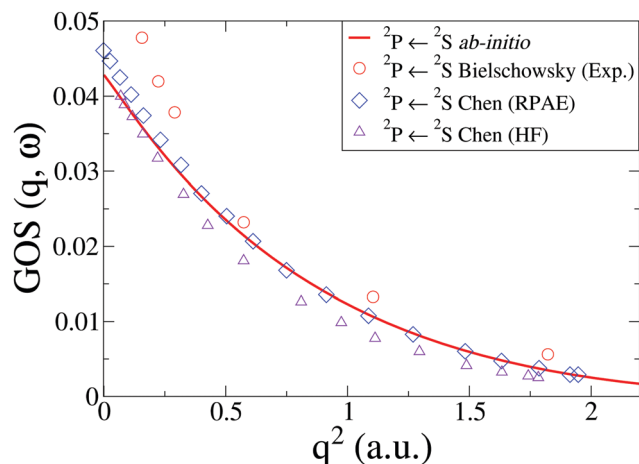

Fig. 6 The generalized oscillator strength, GOS(q,ω), in Na for the $^2P(2s^22p^53s^2) \leftarrow\ ^2S(2s^22p^63s)$ transition. The ab initio calculations using CASSCF(11,9)/aug-cc-PVQZ are compared to experiments by Bielschowsky[62] and theory by Chen and Msezane.[61]

0.1130, respectively, which agrees reasonably well with the experimental values of 0.0634 and 0.0718,[63] as well as previous theory.[61] Further improvements in the oscillator strength would most likely require CASPT2 level corrections.

In Na, we have done the calculations at the CASSCF(11,9)/aug-cc-PVQZ level of theory. We consider an inner shell excitation from the doublet ground state, i.e. the $^2P([He]2s^22p^53s^2) \leftarrow\ ^2S([He]2s^22p^63s)$ transition, which has a very low oscillator strength compared to outer electron excitations. The cross sections, shown in Fig. 6 compare well to previous theory at the HF and RPAE level[61] and EELS experiments by Bielschowsky et al.[62]

4.4 Molecules

Finally, we demonstrate that our codes can also calculate IXS cross sections in molecules. We consider the nitrogen molecule, N_2, which is a major component in the earth atmosphere and has an important valence dipole forbidden transition at 9.3 eV that has been studied extensively.[42] This quadrupole allowed transition, called the Lyman–Birge–Hopfield band, corresponds to the $a^1\Pi_g \leftarrow X^1\Sigma_g^+$ transition. Previous theoretical calculations include Tamm–Dancoff (TDA) and random-phase (RPA) approximations by Szabo and Ostlund,[51] Hartree–Fock calculations by Chung and Lin,[66] and more recent CAS and MRCI calculations by Giannerini et al.[65] and TD-DFT by Sakko et al.[67] These complement a large number of experimental studies.[5,6,42,64,68]

Bradley et al.[5] have identified deviations from first Born approximation scattering in the EELS signal at high q by comparison to IXS, along the lines of similar observations in Ne discussed earlier. A detailed analysis of TD-DFT theory and experiments in ref. 6, shows further that the $a^1\Pi_g \leftarrow X^1\Sigma_g^+$ transition occurs in a region where there are additional contributions from the octupolar $w^1\Delta_u \leftarrow X^1\Sigma_g^+$ transition in the experimental signal, although in the following we focus on the transition to the $a^1\Pi_g$ state.

The energy for the transition obtained using SA-CASSCF(14,12)/aug-cc-PVCTZ is within 0.3% of the experimental[42] value.

Table 4 Energy E for the $a^1\Pi_g$ state in N_2, corresponding to the transition energy from the $X^1\Sigma_g^+$ ground state. The experimental result is taken from Leung et al.[42] Ab initio CASSCF(14,12) and MRCI(14,10) results are shown, using the Dunning Rydberg-adapted aug-cc-PVCTZ basis. The percentage error, ΔE, compared to the experimental value is also given

N_2	E (eV)	ΔE (%)
Exp.[42]	9.300	—
CASSCF(14,12)	9.332	0.3
MRCI(14,10)	9.700	4.3

Table 4 shows the experimental and theoretical energies E for the $a^1\Pi_g$ state in N_2, as well as the percentage error, ΔE, compared to experimental values from Leung.[42] Also included are the results for a MRCI(14,10)/aug-cc-PVCTZ calculation, which in principle should perform better than CASSCF, but due to computational problems had to be run at lower symmetry which adversely affected the energy convergence.

The generalized oscillator strength, $GOS(q,\omega)$, that we have calculated is in good agreement with the experimental results from Leung et al.[42] and Barbieri et al.,[64] shown in Fig. 7, as well as recent theoretical calculations by Giannerini.[65] The MRCI results provide a slightly lower scattering cross section, but the difference is small. The calculated cross sections are below the experiments at high values of q. As discussed above, in terms of comparison to EELS the reason for this difference is primarily the failure of the first Born approximation in EELS. For IXS the discrepancy is smaller, and is due to additional contributions from the $w^1\Delta_u$ state in the Lyman–Birge–Hopfield band.[6]

Finally, a brief remark regarding the energy convergence of the ab initio calculations, as summarized in Tables 1–4. In C and Na the number of Slater determinants is restricted to correctly isolate the inner-shell transitions considered, which impacts on the treatment of electron correlation. The valence transition considered in N_2 allows for greater flexibility in the choice of active space, leading to a good account of static electron correlation, with the calculation close to full CI.
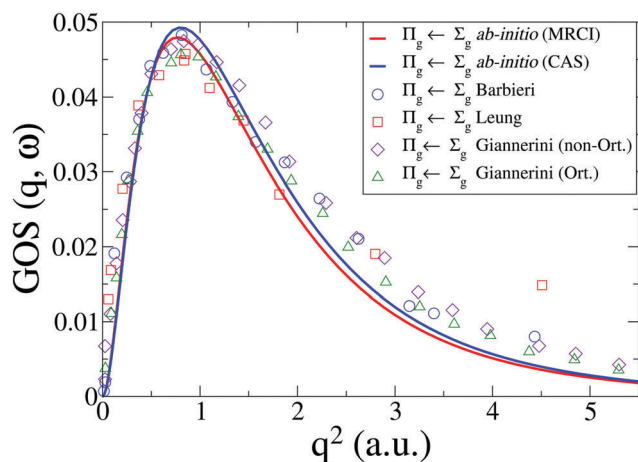

Fig. 7 Generalized oscillator strength, $GOS(q,\omega)$, for the $a^1\Pi_g \leftarrow X^1\Sigma_g^+$ transition in N_2. Our CASSCF and MRCI ab initio results are compared to experimental results from Leung et al.[42] and Barbieri et al.,[64] and to calculations by Giannerini et al.[65]

5 Conclusions

We have calculated a wide range of inelastic scattering cross sections, including inner-shell and valence transitions in closed and open shell atoms, and a benchmark transition in the N_2 molecule. We find good agreement with experimental data from IXS and EELS, and agreement with exact theory for the H and He^+ atoms and previous calculations. In terms of the $L_{\beta\alpha}$ off-diagonal matrix elements, a range of different computational techniques is now available. At the highly accurate end, R-matrix and RPAE based methods perform very well for calculations in single atoms, while for large systems TD-DFT strikes the necessary balance between computational cost and accuracy.[67] However, TD-DFT is generally not appropriate for the simulation of complex photochemical reactions in isolated molecules, and is known to yield results that are quite divergent from established reaction paths.[69]

The approach presented in this paper covers the ground between these two extremes. It calculates inelastic scattering matrix elements at a level of ab initio theory congruent with state-of-the-art quantum molecular dynamics simulations, and is therefore well placed to evaluate inelastic contributions to the signals observed in ultrafast X-ray scattering experiments.[31] As discussed in the Introduction, an important motivation for this work is the prospect of identifying electronic transitions in time-dependent ultrafast X-ray scattering experiments, which could enable complete characterization of reaction paths using X-ray scattering. Achieving the same insights today requires the combination of ultrafast X-ray scattering with a different experimental technique, e.g. time-resolved photoelectron spectroscopy.[70] Finally, the accuracy of the matrix elements calculated by our method is only limited by the quality of the ab initio wavefunctions, and can be systematically improved by adjustments of the ab initio method and basis. Our approach involves a direct summation over all multipole matrix elements, aiding immediate comparison to experiments.

The link between IXS and EELS suggests that the codes developed here could be useful for detailed analysis of ultrafast electron diffraction (UED) data, as long as the nuclear-scattering contribution is included in the elastic terms.[71] Future extensions of this work would be to include the effect of nuclear motion in the IXS signal, as we have recently done for elastic scattering,[37,38] and to consider Compton ionization by the inclusion of continuum states either via multichannel quantum defect formalism[72–74] or a Dyson orbital approach.[75] We also aim to examine in greater detail the mapping of the wavefunction in momentum space made possible by inelastic measurements.

Acknowledgements

This journal is © the Owner Societies 2017

Phys. Chem. Chem. Phys., 2017, **19**, 19545–19553 | **19551**

References

1 D. McMorrow and J. Als-Nielsen, *Elements of Modern X-Ray Physics*, Wiley-Blackwell, 2nd edn, 2011.

2 W. Schülke, *Electron Dynamics by Inelastic X-Ray Scattering*, Oxford Science Publications, 1st edn, 2007.

3 M. Minzer, J. A. Bradley, R. Musgrave, G. T. Seidler and A. Skilton, *Rev. Sci. Instrum.*, 2008, **79**, 086101.

4 R. Verbeni, T. Pylkkänen, S. Huotari, L. Simonelli, G. Vankó, K. Martel, C. Henriquet and G. Monaco, *J. Synchrotron Radiat.*, 2009, **16**, 469–476.

5 J. A. Bradley, G. T. Seidler, G. Cooper, M. Vos, A. P. Hitchcock, A. P. Sorini, C. Schlimmer and K. P. Nagle, *Phys. Rev. Lett.*, 2010, **105**, 053202.

6 J. A. Bradley, A. Sakko, G. T. Seidler, A. Rubio, M. Hakala, K. Hämäläinen, G. Cooper, A. P. Hitchcock, K. Schlimmer and K. P. Nagle, *Phys. Rev. A: At., Mol., Opt. Phys.*, 2011, **84**, 022510.

7 B. Xie, L. Zhu, K. Yang, B. Zhou, N. Hiraoka, Y. Cai, Y. Yao, C. Wu, E. Wang and D. Feng, *Phys. Rev. A: At., Mol., Opt. Phys.*, 2010, **82**, 032501.

8 L. Zhu, L. Wang, B. Xie, K. Yang, N. Hiraoka, Y. Cai and D. Feng, *J. Phys. B: At., Mol. Opt. Phys.*, 2011, **44**, 025203.

9 X. Kang, K. Yang, Y. W. Liu, W. Q. Xu, N. Hiraoka, K. D. Tsuei, P. F. Zhang and L. F. Zhu, *Phys. Rev. A: At., Mol., Opt. Phys.*, 2012, **86**, 022509.

10 L. F. Zhu, W. Q. Xu, K. Yang, Z. Jiang, X. Kang, B. P. Xie, D. L. Feng, N. Hiraoka and K. D. Tsuei, *Phys. Rev. A: At., Mol., Opt. Phys.*, 2012, **85**, 030501.

11 Y.-G. Peng, X. Kang, K. Yang, X.-L. Zhao, Y.-W. Liu, X.-X. Mei, W.-Q. Xu, N. Hiraoka, K.-D. Tsuei and L.-F. Zhu, *Phys. Rev. A: At., Mol., Opt. Phys.*, 2014, **89**, 032512.

12 Y.-W. Liu, X.-X. Mei, X. Kang, K. Yang, W.-Q. Xu, Y.-G. Peng, N. Hiraoka, K.-D. Tsuei, P.-F. Zhang and L.-F. Zhu, *Phys. Rev. A: At., Mol., Opt. Phys.*, 2014, **89**, 014502.

13 J. N. Galayda, J. Arthur, D. F. Ratner and W. E. White, *J. Opt. Soc. Am. B*, 2010, **27**, B106.

14 A. Barty, J. Küpper and H. N. Chapman, *Annu. Rev. Phys. Chem.*, 2013, **64**, 415.

15 C. Bostedt, J. D. Bozek, P. H. Bucksbaum, R. N. Coffee, J. B. Hastings, Z. Huang, R. W. Lee, S. Schorb, J. N. Corlett, P. Denes, P. Emma, R. W. Falcone, R. W. Schoenlein, G. Doumy, E. P. Kanter, B. Kraessig, S. Southworth, L. Young, L. Fang, M. Hoener, N. Berrah, C. Roedig and L. F. DiMauro, *J. Phys. B: At., Mol. Opt. Phys.*, 2013, **46**, 164003.

16 J. Feldhaus, M. Krikunova, M. Meyer, T. Möller, R. Moshammer, A. Rudenko, T. Tschentscher and J. Ullrich, *J. Phys. B: At., Mol. Opt. Phys.*, 2013, **46**, 164002.

17 M. Yabashi, H. Tanaka, T. Tanaka, H. Tomizawa, T. Togashi, M. Nagasono, T. Ishikawa, J. R. Harries, Y. Hikosaka, A. Hishikawa, K. Nagaya, N. Saito, E. Shigemasa, K. Yamanouchi and K. Ueda, *J. Phys. B: At., Mol. Opt. Phys.*, 2013, **46**, 164001.

18 V. Lyamayev, Y. Ovcharenko, R. Katzy, M. Devetta, L. Bruder, A. LaForge, M. Mudrich, U. Person, F. Stienkemeier, M. Krikunova, T. Möller, P. Piseri, L. Avaldi, M. Coreno, P. O'Keeffe, P. Bolognesi, M. Alagia, A. Kivimäki, M. D. Fraia, N. B. Brauer, M. Drabbels, T. Mazza, S. Stranges, P. Finetti, C. Grazioli, O. Plekan, R. Richter, K. C. Prince and C. Callegari, *J. Phys. B: At., Mol. Opt. Phys.*, 2013, **46**, 164007.

19 J. Choi, J. Y. Huang, H. S. Kang, M. G. Kim, C. M. Yim, T.-Y. Lee, J. S. Oh, Y. W. Parc, J. H. Park, S. J. Park, I. S. Ko and Y. J. Kim, *J. Korean Phys. Soc.*, 2007, **50**, 1372.

20 M. P. Minitti, J. M. Budarz, A. Kirrander, J. S. Robinson, D. Ratner, T. J. Lane, D. Zhu, J. M. Glownia, M. Kozina, H. T. Lemke, M. Sikorski, Y. Feng, S. Nelson, K. Saita, B. Stankus, T. Northey, J. B. Hastings and P. M. Weber, *Phys. Rev. Lett.*, 2015, **114**, 255501.

21 M. P. Minitti, J. M. Budarz, A. Kirrander, J. Robinson, T. J. Lane, D. Ratner, K. Saita, T. Northey, B. Stankus, V. Cofer-Shabica, J. Hastings and P. M. Weber, *Faraday Discuss.*, 2014, **171**, 81.

22 J. M. Budarz, M. P. Minitti, D. V. Cofer-Shabica, B. Stankus, A. Kirrander, J. B. Hastings and P. M. Weber, *J. Phys. B: At., Mol. Opt. Phys.*, 2016, **49**, 034001.

23 B. Stankus, J. M. Budarz, A. Kirrander, D. Rogers, J. Robinson, T. J. Lane, D. Ratner, J. Hastings, M. P. Minitti and P. M. Weber, *Faraday Discuss.*, 2016, **194**, 525–536.

24 J. M. Glownia, A. Natan, J. P. Cryan, R. Hartsock, M. Kozina, M. P. Minitti, S. Nelson, J. Robinson, T. Sato, T. van Driel, G. Welch, C. Weninger, D. Zhu and P. H. Bucksbaum, *Phys. Rev. Lett.*, 2016, **117**, 153003.

25 K. H. Kim, J. G. Kim, S. Nozawa, T. Sato, K. Y. Oang, T. W. Kim, H. Ki, J. Jo, S. Park, C. Song, T. Sato, K. Ogawa, T. Togashi, K. Tono, M. Yabashi, T. Ishikawa, J. Kim, R. Ryoo, J. Kim, H. Ihee and S. I. Adachi, *Nature*, 2015, **518**, 385.

26 R. S. Minns and A. Kirrander, *Faraday Discuss.*, 2016, **194**, 11–13.

27 R. Neutze, R. Wouts, S. Techert, J. Davidsson, M. Kocsis, A. Kirrander, F. Schotte and M. Wulff, *Phys. Rev. Lett.*, 2001, **87**, 195508.

28 N. E. Henriksen and K. B. Møller, *J. Phys. Chem. B*, 2008, **112**, 558.

29 U. Lorenz, K. B. Møller and N. E. Henriksen, *Phys. Rev. A: At., Mol., Opt. Phys.*, 2010, **81**, 023422.

30 K. B. Møller and N. E. Henriksen, *Struct. Bonding*, 2012, **142**, 185.

31 A. Kirrander, K. Saita and D. V. Shalashilin, *J. Chem. Theory Comput.*, 2016, **12**, 957–967.

32 G. Dixit, O. Vendrell and R. Santra, *Proc. Natl. Acad. Sci. U. S. A.*, 2012, **109**, 11636.

33 G. Dixit and R. Santra, *J. Chem. Phys.*, 2013, **138**, 134311.

34 H. J. Suominen and A. Kirrander, *Phys. Rev. Lett.*, 2014, **112**, 043002.

35 H. J. Suominen and A. Kirrander, *Phys. Rev. Lett.*, 2014, **113**, 189302.

36 T. Northey, N. Zotev and A. Kirrander, *J. Chem. Theory Comput.*, 2014, **10**, 4911.

37 T. Northey, A. M. Carrascosa, S. Schäfer and A. Kirrander, *J. Chem. Phys.*, 2016, **145**, 154304.

19552 | *Phys. Chem. Chem. Phys.*, 2017, **19**, 19545–19553

This journal is © the Owner Societies 2017

38 A. M. Carrascosa, T. Northey and A. Kirrander, *Phys. Chem. Chem. Phys.*, 2017, **19**, 7853–7863.

39 I. Waller and D. R. Hartree, *Proc. R. Soc. London, Ser. A*, 1929, **124**, 119.

40 P. Eisenberger and P. M. Platzman, *Phys. Rev. A: At., Mol., Opt. Phys.*, 1970, **2**, 415–423.

41 A. Debnarova and S. Techert, *J. Chem. Phys.*, 2006, **125**, 224101.

42 K. T. Leung, *J. Electron Spectrosc. Relat. Phenom.*, 1999, **100**, 237–257.

43 H. Bethe, *Ann. Phys.*, 1930, **397**, 325–400.

44 M. Inokuti, *Rev. Mod. Phys.*, 1971, **43**, 297–347.

45 I. E. McCarthy and E. Weigold, *Rep. Prog. Phys.*, 1991, **54**, 789.

46 M. Y. Amusia, L. V. Chernysheva, Z. Felfli and A. Z. Msezane, *Phys. Rev. A: At., Mol., Opt. Phys.*, 2002, **65**, 062705.

47 L.-F. Zhu, H.-C. Tian, Y.-W. Liu, X. Kang and G.-X. Liu, *Chin. Phys. B*, 2015, **24**, 43101.

48 A. Szabo and N. S. Ostlund, *Modern Quantum Chemistry: Introduction to Advanced Electronic Structure Theory*, Dover Publishing Inc., 2nd edn, 1996.

49 H. B. Schlegel and M. J. Frisch, *Int. J. Quantum Chem.*, 1995, **54**, 83–87.

50 A. Kirrander, *J. Chem. Phys.*, 2012, **137**, 154310.

51 A. Szabo and N. S. Ostlund, *Chem. Phys. Lett.*, 1972, **17**, 163–166.

52 D. V. Shalashilin, *Faraday Discuss.*, 2011, **153**, 105.

53 B. G. Levine, J. D. Coe, A. M. Virshup and T. J. Martinez, *Chem. Phys.*, 2008, **347**, 3.

54 D. V. Makhov, W. J. Glover, T. J. Martinez and D. V. Shalashilin, *J. Chem. Phys.*, 2014, **141**, 054110.

55 G. Richings, I. Polyak, K. Spinlove, G. Worth, I. Burghardt and B. Lasorne, *Int. Rev. Phys. Chem.*, 2015, **34**, 269–308.

56 H.-J. Werner, P. J. Knowles, G. Knizia, F. R. Manby and M. Schütz, *et al.*, *MOLPRO, version 2012.1, a package of ab initio programs*.

57 W. Martin and W. Wiese, *Atomic, Molecular and Optical Physics Handbook*, AIP, Woodbury, NY, 1996, ch. 10, p. 135.

58 N. M. Cann and A. J. Thakkar, *J. Electron Spectrosc. Relat. Phenom.*, 2002, **123**, 143–159.

59 L. Gomis, I. Diedhiou, M. S. Tall, S. Diallo, C. S. Diatta and B. Niassy, *Phys. Scr.*, 2007, **76**, 494–500.

60 H.-D. Cheng, L.-F. Zhu, Z.-S. Yuan, X.-J. Liu, J.-M. Sun, W.-C. Jiang and K.-Z. Xu, *Phys. Rev. A: At., Mol., Opt. Phys.*, 2005, **72**, 012715.

61 Z. Chen and A. Z. Msezane, *Phys. Rev. A: At., Mol., Opt. Phys.*, 2004, **70**, 032714.

62 C. E. Bielschowsky, C. A. Lucas, G. G. B. de Souza and J. C. Nogueira, *Phys. Rev. A: At., Mol., Opt. Phys.*, 1991, **43**, 5975–5979.

63 W. L. Wiese, M. W. Smith and B. M. Glennon, *Atomic Transition Probabilities*, Nat. Bur. Stand., Washington, DC, 1966.

64 R. S. Barbieri and R. A. Bonham, *Phys. Rev. A: At., Mol., Opt. Phys.*, 1992, **45**, 7929–7941.

65 T. Giannerini, I. Borges and E. Hollauer, *Phys. Rev. A: At., Mol., Opt. Phys.*, 2007, **75**, 012706.

66 S. Chung and C. C. Lin, *Appl. Opt.*, 1971, **10**, 1790–1794.

67 A. Sakko, A. Rubio, M. Hakala and K. Hämäläinen, *J. Chem. Phys.*, 2010, **133**, 174111.

68 E. Fainelli, R. Camilloni, G. Petrocelli and G. Stefani, *Il Nuovo Cimento D*, 1987, vol. 9, pp. 33–44.

69 O. Schalk, T. Geng, T. Thompson, N. Baluyot, R. D. Thomas, E. Tapavicza and T. Hansson, *J. Phys. Chem. A*, 2016, **120**, 2320–2329.

70 C. C. Pemberton, Y. Zhang, K. Saita, A. Kirrander and P. M. Weber, *J. Phys. Chem. A*, 2015, **119**, 8832.

71 M. Stefanou, K. Saita, D. Shalashilin and A. Kirrander, *Chem. Phys. Lett.*, 2017, DOI: 10.1016/j.cplett.2017.03.007.

72 A. Kirrander, H. H. Fielding and Ch. Jungen, *J. Chem. Phys.*, 2007, **127**, 164301.

73 A. Kirrander, Ch. Jungen and H. H. Fielding, *J. Phys. B: At., Mol. Opt. Phys.*, 2008, **41**, 074022.

74 A. Kirrander, C. Jungen and H. H. Fielding, *Phys. Chem. Chem. Phys.*, 2010, **12**, 8948.

75 C. M. Oana and A. I. Krylov, *J. Chem. Phys.*, 2007, **127**, 234106.

This journal is © the Owner Societies 2017

Phys. Chem. Chem. Phys., 2017, **19**, 19545–19553 | **19553**